Sound absorption of a double-leaf micro-perforated panel with an air-back cavity and a rigid-back wall: Detailed analysis with a Helmholtz-Kirchhoff integral formulation

Sakagami, Kimihiro

Matsutani, Kiyotaka

Morimoto, Masayuki

(Citation)
Applied Acoustics,71(5):411-417

(Issue Date)
2010-05

(Resource Type)
journal article

(Version)
Accepted Manuscript

(URL)
https://hdl.handle.net/20.500.14094/90001282

Sound absorption of a double-leaf microperforated panel with an air-back cavity and a rigid-back wall: Detailed analysis with a Helmholtz-Kirchhoff integral formulation

Kimihiro Sakagami*, Kiyotaka Matsutani, and Masayuki Morimoto

Environmental Acoustics Laboratory, Department of Architecture, Graduate School of Engineering, Kobe University

Rokko, Nada, 657-8501 Kobe, Japan

Keywords: Microperforated panel (MPP), Double-leaf MPP, Sound absorption, Wave theory, Electro-Acoustical equivalent circuit analysis

*Corresponding Author: +81 78 803 6043, saka@kobe-u.ac.jp

ABSTRACT

So far the electro-acoustical equivalent circuit analysis has been widely used to analyse microperforated panel (MPP) absorbers, however, as for the double-leaf MPP the equivalent circuit analysis inevitably includes an approximation. In this paper, the sound absorption characteristics of a double-leaf MPP absorber backed by a rigid wall are analysed by wave theory using Helmholtz-Kirchhoff integral formulation to obtain a strict solution. The present wave theory is experimentally validated with existing measured results. The theory is also compared with the equivalent circuit solutions so that the differences between the two theories appear and the effect of the approximation is clarified. The comparison shows that the difference mainly appears in the vicinity of the resonance peaks: the differences occur in the resonance frequencies and the absorption coefficient at frequencies between the two resonance peaks.

1. INTRODUCTION

Porous sound absorbing materials have been most widely used for sound absorbing purposes so far, however, they have some deficiencies in hygienic problems, durability and recyclability. For the substituting materials, so-called “next-generation sound absorbers”, microperforated panel (MPP) absorbers are now known to be the most promising and applied to various situations [1-9]. MPPs are mainly made out of metal or plastic panels with microperforations of less than 1mm diameter and less than 1 % perforation ratio. Usually MPPs are used by placing with an air-back cavity and a rigid back wall. This setting offers high sound absorptivity at mid- to high-frequencies. Also, MPPs can be made effective in wider frequency range by using two MPPs placed in parallel with an air-cavity and a rigid back wall (double MPPs) [1,2,9].

For the prediction of the absorption characteristics of MPP absorbers, so far electro-acoustical equivalent circuit models have been widely used [1-4,10-12]. However, in the case of double MPP absorbers, in the equivalent circuit theory the impedance of air-layer between two MPPs is often approximated [1,2,10], which leads to a discrepancy between the prediction and experimental results in some frequency ranges [13]. In Ref [13] the impedance transfer method (ITM) is used for double MPPs to develop a new prediction method of the sound absorption characteristics. In the same paper, comparison among the ITM theory, electro-acoustical equivalent circuit and the experimental results is made, and further discussion on relationship between electro-acoustical equivalent circuit model and ITM solutions is given. For a multi-layer absorbing structure including perforated panels, acoustic transmission analysis (ATA) is proposed by Lee and Chen [14]. The ATA method can also offer a better prediction than electro-acoustical equivalent circuit approach for sound absorption characteristics of multi-layer absorbers including perforated panels.

In the present paper, a novel approach to the double MPP absorber by using strict wave theory

based on Helmholtz-Kirchhoff integral formulation [15-18] is proposed. Although ITM and its similar approach can be well used to obtain correct solution for multiple layer absorption structures including double-leaf MPPs, Helmholtz-Kirchhoff integral formulation is more general and expandable, which can be extended to the cases where various other construction (e.g., elastic support, honeycomb in the cavity, etc that will be dealt with in further studies) are included. The present theory is experimentally validated with existing measured results. Using the present theory double MPP absorbers are strictly analysed in detail. The theoretical results will be compared with equivalent circuit model results so that their difference is clarified: this also clarifies the applicability and appropriateness of the electro-acoustical equivalent circuit analyses.

2. THEORETICAL CONSIDERATIONS

2.1 Model

Figure 1 shows a theoretical model of a double MPP absorber with a rigid back wall. Consider a plane wave of unit pressure amplitude is incident at angle θ upon the double MPP absorber in x-y plane. The MPP on the illuminated side is MPP1 and the second MPP is MPP2. The thicknesses, hole diameters, perforation ratios, surface densities, Young's moduli, loss factors, Poisson's ratios and acoustic impedances of MPP1 and MPP2 are respectively $t_{1,2}$, $d_{1,2}$, $p_{1,2}$, $M_{1,2}$, $E_{1,2}$, $\eta_{p1,2}$, $\nu_{1,2}$, $Z_{1,2}$. The thickness of the air-cavity between MPP1 and MPP2 is D_1, and that between MPP2 and the rigid back wall is D_2. MPPs are supposed to be set in vibration by the surrounding wave motion, and this sound–induced vibration is taken into consideration in the present analysis. The displacements of the sound induced vibrations of MPP1 and MPP2 are $w_1(x)$ and $w_2(x)$,. respectively. The time factor is $\exp(-i\omega t)$, and suppressed throughout.

2.2 Acoustic Impedance of an MPP

The relative acoustic impedance of an MPP, z_j, is described by the Maa's formulae as follows [2]:

$$z_j = r_j - i\omega m_j, \qquad j = 1,2 \quad ; \tag{1}$$

$$r_j = \frac{32\eta t_j}{p_j \rho_0 c_0 d_j^{\,2}} \left(\sqrt{1 + \frac{k_j^{\,2}}{32}} + \frac{\sqrt{2}}{32} k_j \frac{d_j}{t_j} \right) \qquad j = 1,2 \tag{2}$$

$$\omega m_j = \frac{\omega t_j}{p_j c_0} \left(1 + \frac{1}{\sqrt{9 + \frac{k_j^{\,2}}{2}}} + 0.85 \frac{d_j}{t_j} \right) \qquad j = 1,2 \tag{3}$$

$$k_j = d_j \sqrt{\frac{\omega \rho_0}{4\eta}} \qquad j = 1,2 \tag{4}$$

where r_j is the resistance and ωm_j is the reactance, which both are normalised to the air impedance $\rho_0 c_0$ (ρ_0 is the air density, and c_0 is the sound speed in the air), ω_0 is the angular frequency, and η is the dynamic viscosity of the air (=1.789×10^{-5}[Pa s])

2.3 Formulation by Helmholtz-Kirchhoff Integrals

Using a Helmholtz-Kirchhoff integral formula the surface pressure on the illuminated side of MPP1 is written, by using a Green's function for two-dimensional sound field $G(r|r_0)=(i/4)\mathrm{H}_0^{(1)}(k_0|r\text{-}r_0|)$, as follows [15]:

$$p_1(x,0) = 2p_i(x,0) + \frac{i}{2}\int_{-\infty}^{\infty} \frac{\partial p_1(x_0)}{\partial n} H_0^{(1)}(k_0|x - x_0|)dx_0 \quad . \tag{5}$$

Here, p_i is the pressure of the incident plane wave, n is the outward normal, and $\mathrm{H}_0^{(1)}$ is the Hankel function of the first kind of order zero. The boundary condition on the surface is as follows [16,17]:

$$\frac{\partial p_1(r_0)}{\partial n} = \rho_0 \omega^2 w_1(x_0) + iA_{m1} k_0 \Delta P_1(x_0) \quad , \tag{6}$$

where, $A_{m1}=\rho_0 c_0/Z_1$, with k_0 the wavenumber, ΔP_1 is the pressure difference between two sides of MPP1. From these equations above, the sound pressure on the illuminated side surface becomes [16,17]:

$$p_1(x,0) = 2p_i(x,0) + \frac{i}{2}\int_{-\infty}^{\infty} [\rho_0 \omega^2 w_1(x_0) + iA_{m1} k_0 \Delta P_1(x_0,0)] H_0^{(1)}(k_0|x-x_0|) dx_0 \quad . \tag{7}$$

The pressures and the particle velocities in the regions 2 and 3 are described as follows, by using the general solution of plane standing waves.

$$p_{2,3}(x,z) = (X_{2,3} e^{ik_0 z\cos\theta} + Y_{2,3} e^{-ik_0 z\cos\theta}) e^{ik_0 x\sin\theta} \quad , \tag{8}$$

$$v_{2,3}(x,z) = \frac{\cos\theta}{\rho_0 c_0} (X_{2,3} e^{ik_0 z\cos\theta} - Y_{2,3} e^{-ik_0 z\cos\theta}) e^{ik_0 x\sin\theta} \quad . \tag{9}$$

The boundary conditions for these pressures and velocities are:

$$v_2(x,0) = -i\omega w_1(x) + \frac{\Delta P_1(x)}{z_1} \quad , \tag{10}$$

$$v_2(x,D_1) = -i\omega w_2(x) + \frac{\Delta P_2(x)}{z_2} \quad , \tag{11}$$

$$v_3(x,D_1) = -i\omega w_2(x) + \frac{\Delta P_2(x)}{z_2} \quad , \tag{12}$$

$$v_3(x,D_1+D_2) = 0 \quad . \tag{13}$$

Here ΔP_2 is the pressure difference between the two sides of MPP2. From eqs (10)-(13) the complex

pressure amplitudes $X_{2,3}$ and $Y_{2,3}$ can be obtained. The surface pressures on the back side (right hand side) of MPP1 and on the illuminated side (left hand side) of MPP2 can be obtained from X_2 and Y_2. The surface pressure on the back side (right hand side) of MPP2 is obtained from X_3 and Y_3.

The displacement of the sound induced vibration of MPP1 and MPP2, $w_{1,2}(x)$, are, by using the unit responses, $u_{1,2}$, of each MPP, expressed by the following equations [15]:

$$w_1(x) = \int_{-\infty}^{\infty} [p_1(\xi,0) - p_2(\xi,0)] u_1(x-\xi) d\xi \ , \tag{14}$$

$$w_2(x) = \int_{-\infty}^{\infty} [p_2(\xi,D_1) - p_3(\xi,D_1)] u_2(x-\xi) d\xi \ . \tag{15}$$

Solving all the equations above with Fourier transform technique, the reflected sound pressure p_r is obtained as follows:

$$p_r(x,z) = \left[1 + \frac{i\rho_0\omega^2\Gamma_1(k_0\sin\theta) - k_0 A_{m1}\Theta_1\{A_1\Gamma_1(k_0\sin\theta) + A_2\Gamma_2(k_0\sin\theta) + A_3\}}{k_0\cos\theta} \right] e^{i[k_0\sin\theta x - k_0\cos\theta z]} \ . \tag{16}$$

Here, $\Gamma_{1,2}$, $\Theta_{1,2}$, $A_{1,2,3}$, $B_{1,2,3}$ are rather complex functions including MPP impedances and air cavity depth:

$$\Gamma_1(k) = \frac{-\Phi_1 A_3 + \Phi_1\Phi_2 A_3 B_2 - \Phi_1\Phi_2 A_2 B_3}{-1 + \Phi_1 A_1 + \Phi_1\Phi_2 A_2 B_1 + \Phi_2 B_2 - \Phi_1\Phi_2 A_1 B_2} , \tag{17}$$

$$\Gamma_2(k) = \frac{-\Phi_1\Phi_2 A_3 B_1 - \Phi_2 B_3 + \Phi_1\Phi_2 A_1 B_3}{-1 + \Phi_1 A_1 + \Phi_1\Phi_2 A_2 B_1 + \Phi_2 B_2 - \Phi_1\Phi_2 A_1 B_2} , \tag{18}$$

where,

$$\Phi_1 = 2\pi U_1(k)\Theta_1, \quad \Phi_2 = 2\pi U_2(k)\Theta_2; \quad \Theta_1 = \frac{1}{2EK}, \quad \Theta_2 = \frac{1}{-K};$$
$$A_1 = 2(I_2 - L)EJ_2 + I_1J_1J_2 + I_1K, \quad A_2 = -(I_2 - I_3)(K + J_1J_2) - 2EI_1J_2, \quad A_3 = -4EJ_2;$$
$$B_1 = 2E(I_2 - L) + I_1J_1, \quad B_2 = -2EI_1 - (I_2 - I_3)J_1, \quad B_3 = -4E;$$
$$C_1 = (e^{i\varphi} - e^{-i\varphi})\cos\theta, \quad C_2 = (e^{2i\varphi} - e^{2i(\varphi+\sigma)})\cos\theta; \quad E = \frac{\rho_0 c_0}{C_1 Z_1}, \quad F_1 = \frac{\rho_0 c_0}{C_1 Z_2}, \quad F_2 = \frac{\rho_0 c_0}{C_2 Z_2};$$
$$G = i\rho_0 c_0 \omega; \quad H_1 = e^{i\varphi} + e^{-i\varphi}, \quad H_2 = e^{2i\varphi} + e^{2i(\varphi+\sigma)};$$
$$I_1 = \frac{2G}{C_1}, \quad I_2 = \frac{H_1 G}{C_1}, \quad I_3 = \frac{H_2 G}{C_2}; \quad J_1 = 1 - EH_1 + M, \quad J_2 = 1 - F_1 H_1 + F_2 H_2;$$
$$K = 4EF_1 - J_1J_2; \quad L = \frac{i\rho_0\omega^2}{\sqrt{k_0{}^2 - k^2}}; \quad M = \frac{k_0 A_{m1}}{\sqrt{k_0 - k^2}}.$$

Here $U_j(k)=1/[2\pi D_j(k^4-k_{Fj}{}^4)]$ (j=1,2) is the Fourier transform of the panels' unit responses $u_j(x)$ [15], with k the wavenumber parameter, $k_{Fj}{}^4=\rho_{pj}t_j/D_j$, ρ_j, the panel's density and D_j the flexural rigidity ($=E_j t_j^3(1-i\eta_j)/[12(1-\nu_j^2)]$; E_j, η_j, and ν_j are the Young's moduli, loss factors and Poisson's ratio) of the panels.

Sound absorption coefficient is obtained from the reflected pressure by:

$$\alpha_\theta = 1 - |p_r|^2. \tag{19}$$

2.4 Analysis by Electro-acoustical Equivalent Circuit Theory

Figure 2 shows the electro-acoustical equivalent circuit model for the MPP sound absorbing system shown in Fig. 1. For the MPPs their acoustical impedances are derived from eqs.(1)-(4). In order to include the effect of the sound induced vibration of the MPPs, MPPs' mass reactances are introduced and connected to their acoustic impedances in parallel [19]. The combined impedances

consisting the acoustical impedances of the MPPs and the MPPs' mass reactances are expressed as follows:

$$z_j' = \left(\frac{1}{z_j} + \frac{1}{-i\omega M_j / \rho_0 c_0} \right)^{-1}, \quad j = 1,2 \tag{20}$$

The acoustic impedances of the air cavities (normalised to the air impedance $\rho_0 c_0$) are described as follows:

$$z_{h1,2} = i \cot(k_0 D_{1,2}) \tag{21}$$

In this electro-acoustical equivalent circuit model the impedance of the air cavity between the two MPPs, z_{h2}, is approximated, just as in most previous studies (e.g., Refs.[1,2,10]), by the impedance of the air cavity backed by a rigid wall. This approximation is widely used but is also a major weak point in such a simple equivalent circuit formulation when it is used for a multi-layer system. Note that the equivalent circuit formulation can be improved by modelling the air cavity using transmission line theory. However, the simple rigid backing approximation, Eq. (21), is retained here to illustrate the differences between the present theory and conventional simple equivalent circuit analysis.

According to Maa's theory [1-3], for oblique incidence with angle of incidence θ, $z'_{1,2}$ is replaced with $z'_{1,2}\cos\theta$ and k_0 is replaced with $k_0\cos\theta$, and the total impedance of this circuit is:

$$z'_{total} = z_1' \cos\theta + \left\{ \frac{1}{i \cot(k_0 D_1 \cos\theta)} + \frac{1}{z_2' \cos\theta + i \cot(k_0 D_2 \cos\theta)} \right\}^{-1} \tag{22}$$

and the absorption coefficient is expressed as:

$$\alpha = 1 - \left| \frac{z'_{total} - 1}{z'_{total} + 1} \right|^2 \tag{23}$$

3. RESULTS AND DISCUSSION

3.1 Experimental Validation of the Wave Theory

In order to validate the wave theory presented in Sec. 2.2, the numerical results calculated by the present wave theory are compared with the existing experimental results [10]. In Ref [10] the MPPs used in the experiments are termed “textile” or “membrane”, therefore, assuming that they are limp, only the mass is considered in the theoretical calculations here. The theoretical results are shown in comparison with the experimental results in Fig. 3. The MPP parameters are shown in Table 1. In the case of normal incidence the comparison is made for the specimen A, and in the case of diffused field absorption coefficient the specimen B is used for comparison. The specimen A has rectangular perforations with sides $l_{1,2}$, therefore the equivalent hole diameter is approximated as $d_{1,2}=2l_{1,2}/\pi^{1/2}$.

In the theoretical calculation, field-incidence-averaged absorption coefficient (averaged over 0 to 78 degrees on a half-sphere) is employed to compare with diffuse field absorption coefficient. As Fig. 3 shows the results by the present wave theory are in good agreement with the experimental results in both normal incidence and diffuse incidence. Thus, the present wave theory is validated.

3.2 Comparison of the Wave Theory with the Electro-acoustical Equivalent Circuit Theory

The present wave theory is now compared with the electro-acoustical equivalent circuit theory including the approximation as described above, to show the effect of the approximation on the results.

3.2.1 In the Case with Sound Induced Vibration Neglected

(a) Normal incidence absorption coefficient

First, in order to concentrate upon the effect of the approximation included in the equivalent circuit theory, a discussion is made under the condition in which the sound induced vibration does not occur. Neglecting the sound induced vibration, the calculations are made by the equivalent circuit theory and the present wave theory, and those results are compared. In order to realise this condition in the calculations, an extremely large value of the surface densities of MPPs are given in the calculations of the both theory. The results are shown in Fig. 4(A).

Regarding the first resonance absorption peak at low frequencies (around 400 Hz), it appears at lower frequencies in the present wave theory than in the equivalent circuit results. On the contrary, regarding the second resonance peak at high frequencies (around 1 kHz), it appears at higher frequencies in the present wave theory than in the equivalent circuit results. Consequently, the frequency gap between the first and the second peaks becomes larger in the wave theory, which leads to lower absorption coefficient at the frequencies between the two peaks: it is lower than the equivalent circuit results by 0.2. Another difference between the two theories is observed at around 2 kHz: there is a sharp peak due to the higher resonance of the air cavity in the present wave theory, but it is not observed in the equivalent circuit results.

The present wave theory differs in two aspects than the electro-acoustical equivalent circuit model: (1) the present wave theory does not use any approximation in air cavities whereas the equivalent circuit model approximates the air gap between two MPPs, and (2) the present wave theory includes bending wave in MPPs caused by the sound induced vibration. In this case the sound induced vibration is neglected, therefore, the above differences are solely caused by the approximation of the air cavity impedance in the equivalent circuit theory. The approximation of the

cavity impedance in the circuit model causes a shift in the resonance frequency of the system, which results in differences in the peak frequencies. Also, the resonance characteristics can be different due to this approximation, and this can result in the difference in the shape of the peak, e.g., broadness of the peak etc.

(b) Field-incidence-averaged absorption coefficient

Next, the effect of the sound incidence condition on the difference between the present wave theory and the equivalent circuit theory is discussed. The result of the present wave theory for field-incidence-averaged absorption coefficient is compared with that obtained by the equivalent circuit model in Fig. 4 (B).

A similar discussion to the normal incidence case can be obtained. The difference between the two theories is somewhat smaller than that observed in the case of normal incidence. These differences are also solely caused by the approximation in the air cavity impedance in the circuit model, as in this case also the sound induced vibration is neglected. However, the tendency of the difference can be said not to change qualitatively due to the condition of the sound incidence.

(c) Parametric study

The difference between the present theory and the electro-acoustical equivalent circuit theory can be changed by changes in the parameters of the sound absorbing system.

Figure 5 shows the effect of the change in the cavity depth in (A) normal incidence and (B) field-incidence averaged cases. Changes in the cavity depths make a change in the cavity impedance, and that can cause a variation in the difference between the two theories. In Fig. 5 the cavity depths are D_1=D_2=75 mm, and in this case the two resonance peaks occur with a smaller frequency separation. Therefore, the dip between the two resonance peaks, which appears in the results by the

present theory, becomes less significant. This results in the smaller difference between the two theories. However, comparing Fig. 5 with Fig. 4, similar tendencies are observed.

Figure 6 shows two calculated examples for field-incidence averaged absorptivity of MPPs with different parameters: (A) an MPP with larger thickness, and (B) an MPP with larger perforation ratio, with other parameters kept the same as Fig. 4. In Fig. 6 (A) the difference is small. On the contrary, in Fig. 6 (B) the difference is considerably large at the frequencies between the two resonance peaks. It is inferred that the change in the MPP parameter causes a change not only in the peak frequencies but in the cavity impedance as well, and thus, the difference between the present theory and the equivalent circuit model can vary with the MPP parameters. However, on the whole, the tendencies of the difference are qualitatively similar in any case.

3.2.2 In the Case with Sound Induced Vibration Included

Although the sound induced vibration was neglected in the preceding section for the virtue of the simplicity, in reality MPP causes vibration due to sound incidence. Therefore, in this section, the difference between the present wave theory and the electro-acoustical equivalent circuit theory is discussed including the sound induced vibration to clarify how the vibration affects the difference.

Figure 7 presents the results calculated by the present wave theory and the electro-acoustical equivalent circuit theory. Fig. 7 (A) shows the normal incidence case, and (B) shows the field-incidence-averaged case. Comparing Fig. 7 with Fig. 4, in both Figs. (A) and (B), the peak value is lower than in the case neglecting the sound induced vibration (Fig. 4). This can be explained by the decrease in the resistance of the MPP due to the sound induced vibration [19,20]. Although the difference due to the sound induced vibration between Figs. 4 and 7 is not very large on the whole, the difference between the two theories becomes somewhat larger at frequencies between the first and the second peaks, and the difference in the case with sound induced vibration included is

slightly larger than the immobile case. This means that the effect of the sound induced vibration is not very large. The differences between the two theories are generally considered to be caused by both the approximation in the air cavity impedance in the circuit model and the manner of considering the sound induced vibration. Considering these facts the primary cause of the difference between the two theories is the approximation of the air cavity impedance.

Regarding the difference in the manner to include the sound induced vibration, the present wave theory includes bending wave motions in the MPPs, whereas the circuit model includes only piston-like motion with the MPPs' masses. Comparing Fig. 4 (A) and Fig. 7 (A), their difference is not large as mentioned above. In these two results only piston-like motion occurs because they are under normal incidence condition. Also we compare Fig. 4 (B) and Fig. 7 (B): In Fig. 7 (B), as it is under the condition of diffuse sound incidence, the bending wave should be included in the result. However, their difference is not very significant as mentioned above. From these facts, it can be stated the effect of the difference due to the bending wave motion in the MPPs is not very significant in these cases. If there is a coincidence effect, there may be its effect in the result by the present wave theory.

Figure 8 shows another example of the comparison between the two theories including the effect of sound induced vibration. In these figures the cavity depths are changed to D_1=D_2=75 mm. In this case also a similar discussion can be obtained as in Fig. 7.

The effect of the sound induced vibration can cause a change in the difference between the two theories, which is dependent largely on the surface density of the MPP leaves. Figure 9 compares the results of the present theory and the equivalent circuit model for MPPs with different surface densities. When the MPP leaves are extremely lightweight (a) the resonance peak becomes lower because of the decrease in the resistance due to the sound induced vibration. In this case the difference between the two theories becomes larger. However, the surface density becomes larger

than 0.5 kg/m^2 the characteristics hardly change with the surface density, and the difference between the two theories is almost unchanged.

Regarding the effect of the MPP parameters on the difference between the two theories, a comparison similar to Fig. 6 is made with the sound induced vibration included. The results are shown in Fig. 10. Comparing those with Fig. 6 it is observed that the tendencies are hardly changed qualitatively, even if the sound induced vibration is included.

Thus, the difference between the present wave theory and the equivalent circuit theory becomes slightly larger by the effect of the sound induced vibration of MPP leaves, although the primary cause of the difference between two theories is the approximation of the cavity impedance in circuit model. However, the tendency of the difference remains the same as in the case neglecting the vibration.

4. CONCLUDING REMARKS

In this paper, the sound absorption of a double MPP absorber with rigid back wall have been formulated by a Helmholtz-Kirchhoff integral and vibration equations. Using the present theory the sound absorption characteristics of a double MPP absorber was analysed. In order to clarify the difference between the present wave theory and the conventional electro-acoustical equivalent circuit theory the following discussion was made through numerical examples.

First, the present wave theory was validated with existing experimental results. Next, the present theory was compared with the equivalent circuit theory to clarify the difference between them. It was found that the difference mainly appears in peak frequencies, in the absorption coefficient between the first and the second peaks, and at high frequencies. The difference between the two theories is mainly attributed to the approximation of the cavity impedance in the circuit theory. The tendency of

these differences does not change due to sound incidence condition, sound induced vibration of MPP leaves, or MPP's mass and perforation parameters. However, the degree of the difference changes by sound induced vibration through the MPP's mass, and the MPP's acoustic properties through MPP's perforation parameters.

ACKNOWLEDGEMENT

This work was in part supported by the Grant for Scientific Research from the Takahashi Industrial and Economic Research Foundation.

REFERENCES

[1] Maa D-Y. Theory and design of microperforated panel sound-absorbing constructions. Scientia Sinica 1975; 17: 55-71.

[2] Maa D-Y. Microperforated-panel wideband absorber. Noise Control Eng. J. 1987; 29: 77-84.

[3] Maa D-Y. Potential of microperforated panel absorber. J Acoust Soc Am 1998; 104: 2861-2866.

[4] Maa D-Y. Practical single MPP absorber. International Journal of Acoustics and Vibration 2007; 12: 3-6.

[5] Fuchs HV, Zha X, Drotleff HD. Creating low-noise environments in communication rooms. Applied Acoustics 2001; 62: 1375-1396.

[6] Zha X, Fuchs HV, Drotleff HD. Improving the acoustic working conditions for musicians in small spaces. Applied Acoustics 2002; 63: 203-221.

[7] Wu MQ. Micro-perforated panels for duct silencing. Noise Control Engineering J. 1997; 45: 69-77.

[8] Kang J, Brocklesby MW. Feasibility of applying micro-perforated absorbers in acoustic window systems. Applied Acoustics 2005; 66: 669-689.

[9] Asdrubali F, Pispola G. Properties of transparent sound-absorbing panels for use in noise barriers. J Acoust Soc Am 2007; 121: 214-221.

[10] Kang J, Fuchs HV. Predicting the absorption of open weave textiles and micro-perforated membranes backed by an air space. Journal of Sound and Vibration 1999; 220:905-920.

[11] Sakagami K, Morimoto M, Koike W. A numerical study of double-leaf microperforated panel absorbers. Applied Acoustics 2006; 67: 609-619.

[12] Sakagami K, Morimoto M, Yairi M. Application of microperforated panel absorbers to room interior surfaces. International Journal of Acoustics and Vibration 2008; 13: 120-124.

[13] Zou J, Shen Y, Yang J, Qiu X. A note on the prediction method of reverberation absorption coefficient of double layer micro-perforated membrane. Applied Acoustics 2006; 67: 106-111.

[14] Lee F-C, Chen W-H. Acoustic transmission analysis of multi-layer absorbers. Journal of Sound and Vibration 2001; 248:621-634.

[15] Sakagami K, Morimoto M, Takahashi D. Acoustic reflection by an elastic plate with infinite extent. Journal of Acoust. Soc. Jpn (E) 1993; 14: 85-90.

[16] Sakagami K, Nakamori T, Morimoto M, Yairi M. Double-leaf microperforated panel space absorbers: A revised theory and detailed analysis. Applied Acoustics (in print).

[17] Takahashi D, Sakagami K, Morimoto M. Acoustic properties of permeable membranes. J Acoust Soc Am 1996; 99:3003–3009.

[18] Horoshenkov K, Sakagami K, Morimoto M. On the dissipation of acoustic energy in a thin, infinite, poroelastic plate. Acta Acustica united with Acustica 2002;88:500-506.

[19] Sakagami K, Morimoto M, Yairi M. A note on the effect of vibration of a microperforated panel on its sound absorption characteristics. Acoust. Science and Technology 2005; 26: 204-207.

[20] Sakagami K, Morimoto M, Yairi M. A note on the relationship between the sound absorption by microperforated panels and panel/membrane-type absorbers. Applied Acoustics 2009;70:1131-1136.

TABLES and TABLE CAPTIONS

Table 1: The parameters of the MPP in the experiment [10] used in the experimental validation (Section 3.1).

Specimen	$t_{1,2}$(mm)	$l_{1,2}$(mm)	$p_{1,2}$(%)	$b_{1,2}$(mm)	$m_{1,2}$(kg/m^2)	D_1(mm)	D_2(mm)
A	0.13	0.18	4.7	0.83	0.13	30	70

Specimen	$t_{1,2}$(mm)	$d_{1,2}$(mm)	$p_{1,2}$(%)	$b_{1,2}$(mm)	$m_{1,2}$(kg/m^2)	D_1(mm)	D_2(mm)
B	0.11	0.2	0.79	2.0	0.14	30	100

FIGURE CAPTIONS

Fig.1 Theoretical model for a double MPP absorber with a rigid back wall

Fig. 2 Electro-acoustical equivalent circuit model for the double MPP absorber in Fig. 1.

Fig. 3 Comparison of the present wave theory and the existing experimental results [10].

Fig. 4 Comparison between the present wave theory and the electro-acoustical equivalent circuit model. Solid line: present wave theory; Dashed line: equivalent circuit model. (A) Normal incidence. (B) Field-incidence averaged. Sound induced vibration of MPP leaves is neglected.
Parameters are $t_{1,2}$=0.3 mm, $d_{1,2}$=0.3 mm, $p_{1,2}$=1.0 %, D_1=50 mm and D_2=100 mm.

Fig. 5 Comparison between the present wave theory and the electro-acoustical equivalent circuit model. Solid line: present wave theory; Dashed line: equivalent circuit model. (A) Normal incidence. (B) Field-incidence averaged. Sound induced vibration of MPP leaves is neglected. Parameters are $t_{1,2}$=0.3 mm, $d_{1,2}$=0.3 mm, $p_{1,2}$=1.0 %, D_1=75 mm and D_2=75 mm.

Fig. 6 Effect of the MPP parameters on the field-incidence averaged absorption coefficient. (A) $t_{1,2}$=1 mm, $d_{1,2}$=0.3 mm, $p_{1,2}$=1 %, (B) $t_{1,2}$=0.3 mm, $d_{1,2}$=0.3 mm, $p_{1,2}$=2 %. D_1=50 mm and D_2=100 mm. Solid line: present wave theory. Dashed line: equivalent circuit model.

Fig. 7 Comparison between the present wave theory and the electro-acoustical equivalent circuit model. Solid line: present wave theory; Dashed line: equivalent circuit model. (A) Normal incidence. (B) Field-incidence averaged. Sound induced vibration of MPP leaves is considered. Parameters are $t_{1,2}$=0.3 mm, $d_{1,2}$=0.3 mm, $p_{1,2}$=1.0 %, $E_{1,2}$=2.0×10^{11}N/m^2, $\eta_{1,2}$=0.01, $\nu_{1,2}$=0.3, $M_{1,2}$=1.0 kg/m^2, D_1=50 mm and D_2=100 mm.

Fig. 8 Comparison between the present wave theory and the electro-acoustical equivalent circuit model. Solid line: present wave theory; Dashed line: equivalent circuit model. (A) Normal incidence.

(B) Field-incidence averaged. Sound induced vibration of MPP leaves is considered. Parameters are $t_{1,2}$=0.3 mm, $d_{1,2}$=0.3 mm, $p_{1,2}$=1.0 %, $E_{1,2}$=2.0×10^{11}N/m^2, $\eta_{1,2}$=0.01,$\nu_{1,2}$=0.3, $M_{1,2}$=1.0 kg/m^2, and D_1= D_2=75 mm.

Fig. 9 Effect of surface density on the field-incidence averaged absorption coefficient of double-leaf a micro-perforated panel absorber with $t_{1,2}$=0.3 mm, $d_{1,2}$=0.3 mm, $p_{1,2}$=1 %, $E_{1,2}$=2.0×10^{11}N/m^2, $\eta_{1,2}$=0.01, $\nu_{1,2}$=0.3, D_1=50 mm and D_2=100 mm. Surface densities are $M_{1,2}$= (a)0.1, (b)0.3, (c)3.0, and (d)5.0 kg/m^2. Solid line: present wave theory. Dashed line: equivalent circuit model.

Fig. 10 Effect of the MPP parameters on the field-incidence averaged absorption coefficient. (A) t_1=t_2=1 mm, d_1=d_2=0.3 mm, p_1=p_2=1 %, (B) t_1=t_2=0.3 mm, d_1=d_2=0.3 mm, p_1=p_2=2 %, $E_{1,2}$=2.0×10^{11} N/m^2, $\eta_{1,2}$=0.01, $\nu_{1,2}$=0.3, $M_{1,2}$= 1.0 kg/m^2, D_1=50 mm and D_2=100 mm. Solid line: present wave theory. Dashed line: equivalent circuit model.

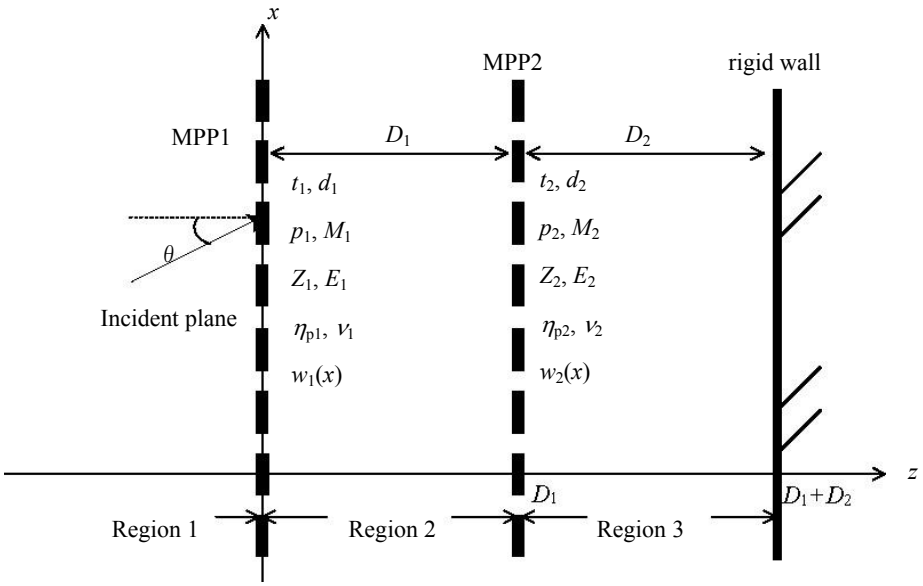

Fig.1 Theoretical model for a double MPP absorber with a rigid back wall

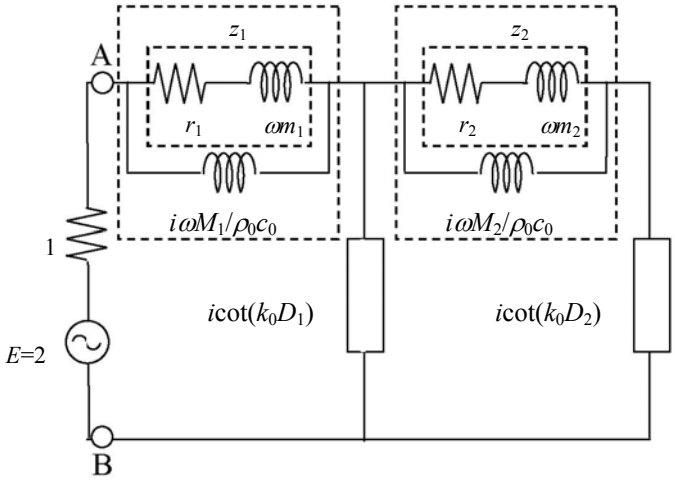

Fig. 2 Electro-acoustical equivalent circuit model for the double MPP absorber in Fig. 1.

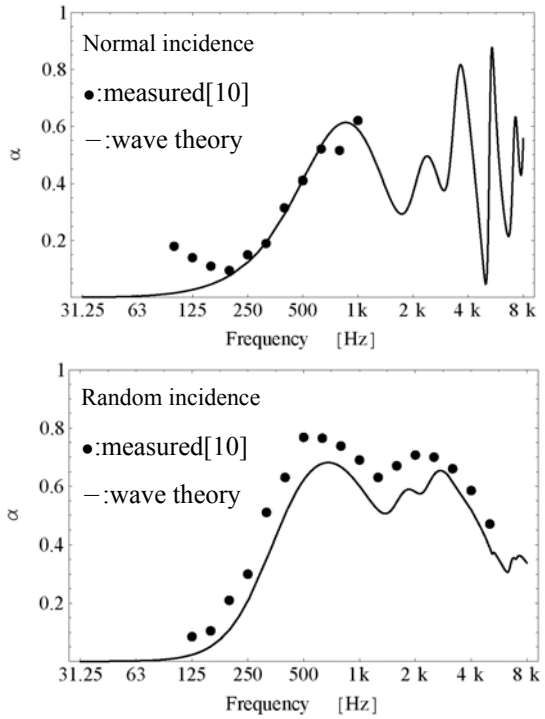

Fig. 3 Comparison of the present wave theory and the existing experimental results [10].

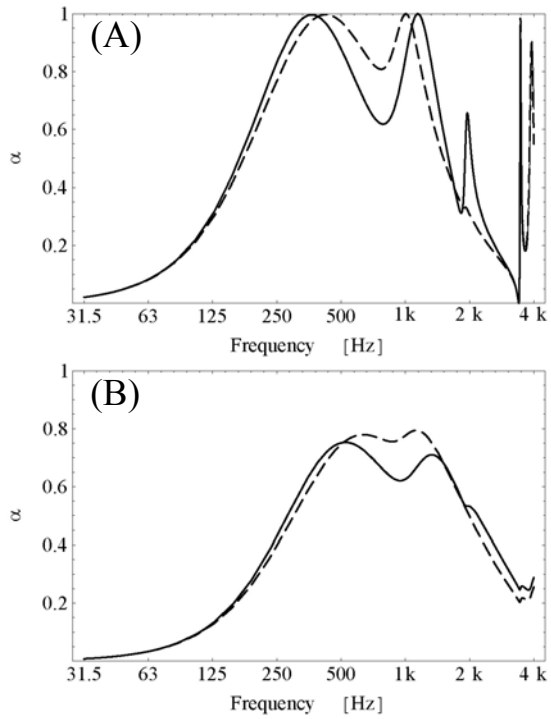

Fig. 4 Comparison between the present wave theory and the electro-acoustical equivalent circuit model. Solid line: present wave theory; Dashed line: equivalent circuit model. (A) Normal incidence. (B) Field-incidence averaged. Sound induced vibration of MPP leaves is neglected. Parameters are $t_{1,2}$=0.3 mm, $d_{1,2}$=0.3 mm, $p_{1,2}$=1.0 %, D_1=50 mm and D_2=100 mm.

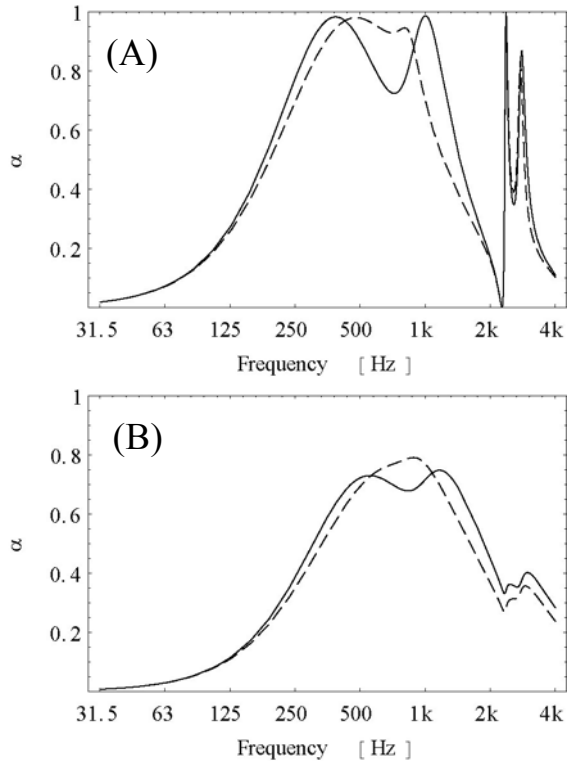

Fig. 5 Comparison between the present wave theory and the electro-acoustical equivalent circuit model. Solid line: present wave theory; Dashed line: equivalent circuit model. (A) Normal incidence. (B) Field-incidence averaged. Sound induced vibration of MPP leaves is neglected. Parameters are $t_{1,2}$=0.3 mm, $d_{1,2}$=0.3 mm, $p_{1,2}$=1.0 %, and D_1= D_2=75 mm.

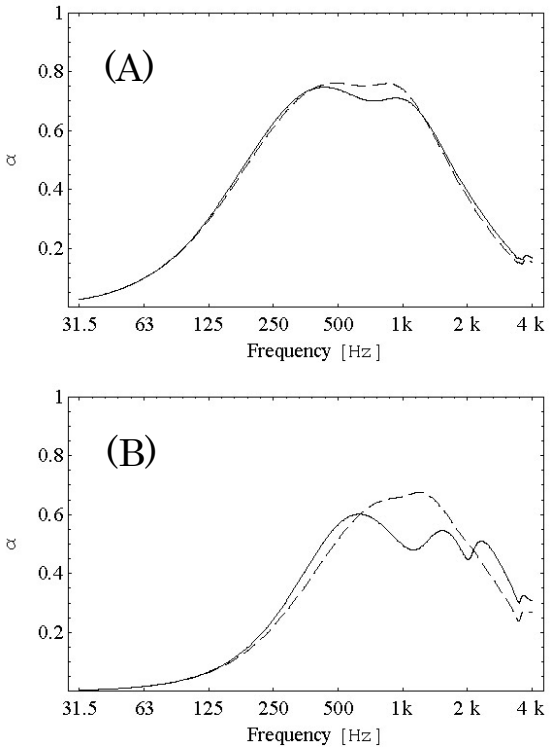

Fig. 6 Effect of the MPP parameters on the field-incidence averaged absorption coefficient. (A) $t_{1,2}$=1 mm, $d_{1,2}$=0.3 mm, $p_{1,2}$=1 %, (B) $t_{1,2}$=0.3 mm, $d_{1,2}$=0.3 mm, $p_{1,2}$=2 %. D_1=50 mm and D_2=100 mm. Solid line: present wave theory. Dashed line: equivalent circuit model.

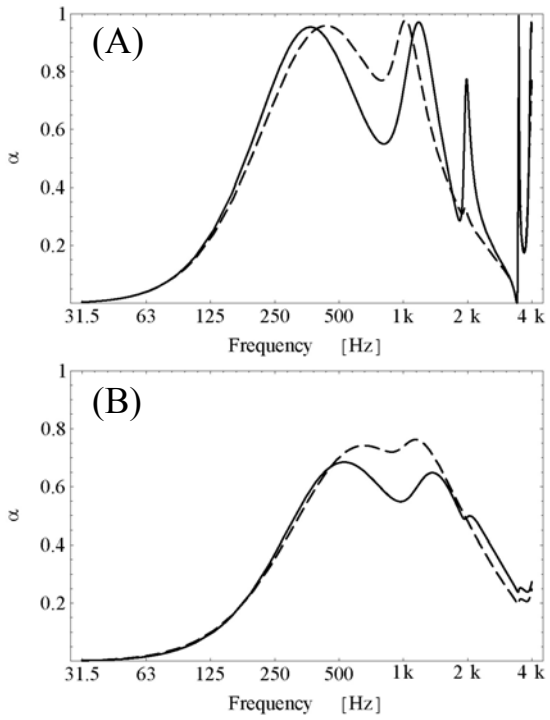

Fig. 7 Comparison between the present wave theory and the electro-acoustical equivalent circuit model. Solid line: present wave theory; Dashed line: equivalent circuit model. (A) Normal incidence. (B) Field-incidence averaged. Sound induced vibration of MPP leaves is considered. Parameters are $t_{1,2}$=0.3 mm, $d_{1,2}$=0.3 mm, $p_{1,2}$=1.0 %, $E_{1,2}$=2.0×10^{11}N/m^2, $\eta_{1,2}$=0.01, $\nu_{1,2}$=0.3, $M_{1,2}$=1.0 kg/m^2, D_1=50 mm and D_2=100 mm.

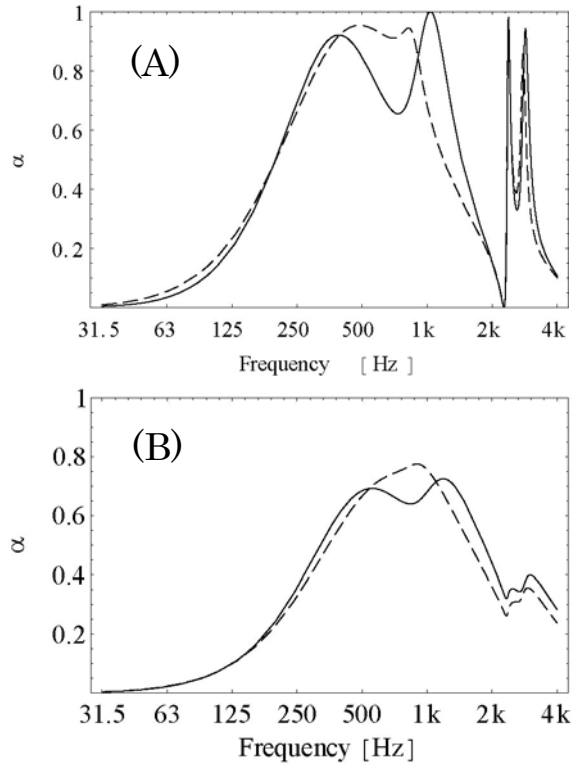

Fig. 8 Comparison between the present wave theory and the electro-acoustical equivalent circuit model. Solid line: present wave theory; Dashed line: equivalent circuit model. (A) Normal incidence. (B) Field-incidence averaged. Sound induced vibration of MPP leaves is considered. Parameters are $t_{1,2}$=0.3 mm, $d_{1,2}$=0.3 mm, $p_{1,2}$=1.0 %, $E_{1,2}$=2.0×10^{11}N/m^2, $\eta_{1,2}$=0.01,$\nu_{1,2}$=0.3, $M_{1,2}$=1.0 kg/m^2, and D_1= D_2=75 mm.

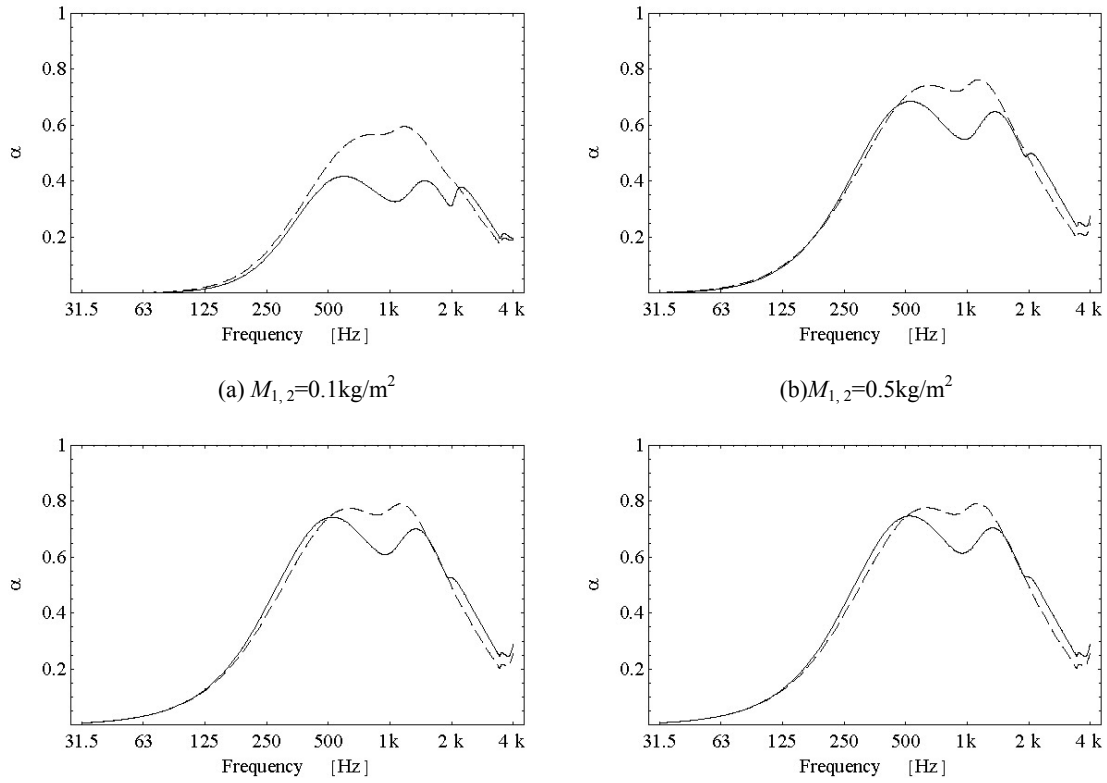

(a) $M_{1,2}$=0.1kg/m^2 (b)$M_{1,2}$=0.5kg/m^2

(c)$M_{1,2}$=3.0kg/m^2 (d) $M_{1,2}$=5.0kg/m^2

Fig. 9 Effect of surface density on the field-incidence averaged absorption coefficient of double-leaf a micro-perforated panel absorber with $t_{1,2}$=0.3 mm, $d_{1,2}$=0.3 mm, $p_{1,2}$=1 %, $E_{1,2}$=2.0×10^{11}N/m^2, $\eta_{1,2}$=0.01, $\nu_{1,2}$=0.3, D_1=50 mm and D_2=100 mm. Surface densities are $M_{1,2}$= (a)0.1, (b)0.3, (c)3.0, and (d)5.0 kg/m^2. Solid line: present wave theory. Dashed line: equivalent circuit model.

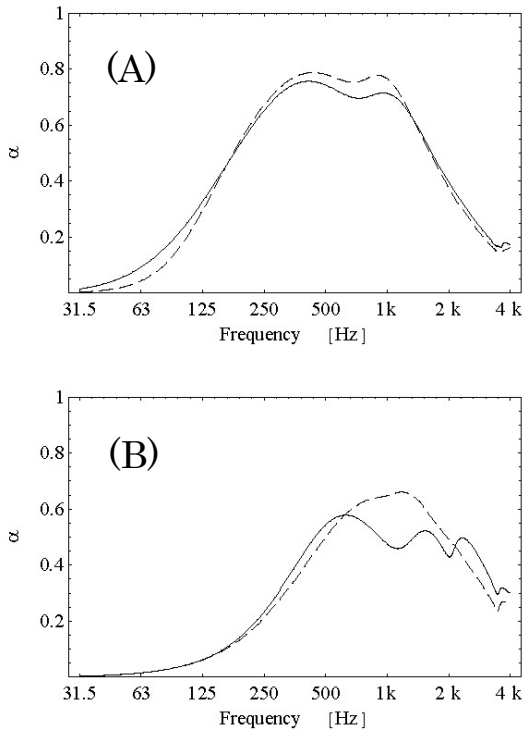

Fig. 10 Effect of the MPP parameters on the field-incidence averaged absorption coefficient. (A) t_1=t_2=1 mm, d_1=d_2=0.3 mm, p_1=p_2=1 %, (B) t_1=t_2=0.3 mm, d_1=d_2=0.3 mm, p_1=p_2=2 %, $E_{1,2}$=2.0×10^{11} N/m^2, $\eta_{1,2}$=0.01, $\nu_{1,2}$=0.3, $M_{1,2}$= 1.0 kg/m^2, D_1=50 mm and D_2=100 mm. Solid line: present wave theory. Dashed line: equivalent circuit model.